Controlling the Binding Efficiency of Surface Confined Antibodies through the Design of Mixed Self-Assembled Monolayers

Sarcina, Lucia; Delre, Pietro; Graziano, Giovanni; Stefanachi, Angela; Blasi, Davide; Picca, Rosaria A.; Di Franco, Cinzia; Leonetti, Francesco; Scamarcio, Gaetano; Bollella, Paolo; Mangiatordi, Giuseppe F.; Macchia, Eleonora; Torsi, Luisa

Published in:
Advanced Materials Interfaces

DOI:
10.1002/admi.202300017

Published: 24/04/2023

Document Version
Final published version

Document License
CC BY

ADVANCED MATERIALS INTERFACES
Open Access
www.advmatinterfaces.de

Controlling the Binding Efficiency of Surface Confined Antibodies through the Design of Mixed Self-Assembled Monolayers

Lucia Sarcina, Pietro Delre, Giovanni Graziano, Angela Stefanachi, Davide Blasi, Rosaria A. Picca, Cinzia Di Franco, Francesco Leonetti, Gaetano Scamarcio, Paolo Bollella, Giuseppe F. Mangiatordi, Eleonora Macchia,* and Luisa Torsi**

A plethora of different electronic and optoelectronic devices have been developed lately, for biosensing applications (e.g., label-free, fast, and easier to operate) based on a detecting interface accommodating the biorecognition elements, anchored by thiolate self-assembled monolayers (SAMs) on a gold surface. Here, a surface plasmon resonance (SPR) characterization of anti-p24 anchored on different SAMs is performed to investigate the effect of the SAM structure on the antibodies' packing efficiency and the sensors' analytical figures of merit. Notably, the mixed SAM deposited from a solution 10:1 of 3-mercaptopropionic acid and 11-mercaptoundecanoic acid (11MUA) is compared to that resulting from a solution 10:1 of ad hoc synthesized *N*-(2-hydroxyethyl)-3-mercaptopropanamide (NMPA)/11MUA. Despite the improvement in the anti-p24 surface coverage registered using the 11MUA/NMPA SAM, the latter produces a significant decrease in the antibodies' binding efficiency against human immunodeficiency virus p24 protein. To provide a molecular rationale behind the SPR data, density functional theory calculations are also undertaken. A comprehensive physical view of the main competing phenomena affecting the biorecognition events at a biofunctionalized gold detecting interface is represented here.

1. Introduction

Recently, the development of ultrasensitive biosensors has experienced tremendous growth, as they have been proven able to accomplish label-free detections, down to the single-molecule ultimate limit with large micrometer/millimeter wide bioelectronic devices based on field-effect-transistor transducers.[1–7] These are high-performing, stable, and reliable systems that exhibit most ideal features to conveniently serve in point-of-care testing systems.[8–10] This technology relies on the integration of biotic components (e.g., proteins, DNA, or RNA) with an abiotic counterpart (e.g., electrodes, devices, or electronic components).[6,11–15] In such devices, the immobilization strategy of the biotic component is of paramount importance. Particularly, those assays often involve the presence of gold-based detecting interfaces.[16–19] In this case,

L. Sarcina, D. Blasi, R. A. Picca, P. Bollella, L. Torsi
Dipartimento di Chimica
Università degli Studi di Bari Aldo Moro
Bari 70126, Italy
E-mail: luisa.torsi@uniba.it

P. Delre, G. F. Mangiatordi
CNR—Institute of Crystallography
Via Amendola 122/o, Bari 70126, Italy
E-mail: giuseppe.mangiatordi@ic.cnr.it

The ORCID identification number(s) for the author(s) of this article can be found under https://doi.org/10.1002/admi.202300017.

DOI: 10.1002/admi.202300017

G. Graziano, A. Stefanachi, F. Leonetti, E. Macchia
Dipartimento di Farmacia-Scienze del Farmaco
Università degli Studi di Bari Aldo Moro
Bari 70126, Italy
E-mail: Eleonora.macchia@uniba.it

C. Di Franco
CNR—Institute of Photonics and Nanotechnologies
Bari 70126, Italy

G. Scamarcio
Dipartimento Interateneo di Fisica "M. Merlin"
Università degli Studi di Bari Aldo Moro
Bari 70126, Italy

G. Scamarcio, P. Bollella, E. Macchia, L. Torsi
Centre for Colloid and Surface Science
Università degli Studi di Bari Aldo Moro
Bari 70126, Italy

E. Macchia, L. Torsi
The Faculty of Science and Engineering
Åbo Akademi University
Turku 20500, Finland

functionalization protocols, encompassing covalent bonding of biorecognition elements through thiol chemistry, are the most widespread approaches.[20–22] In particular, self-assembled monolayers (SAMs) with short- and long-chain carboxylic acid-terminating alkanethiols have been extensively investigated to achieve packed and functional immobilization of biorecognition elements on the gold surface.[1,17,20] Notably, a solution of two distinct alkyl thiols with different aliphatic chain lengths with a molar ratio of 1:10 (11-mercaptoundecanoic acid, 11-MUA/3-mercaptopropionic acid, 3-MPA) has been proven to offer among the highest immobilization efficiency, as it allows improving accessibility for protein binding due to a reduced steric hindrance.[23] The longer chain (i.e., 11-MUA) serves to anchor the biorecognition element and is used in a more diluted concentration, whereas the shorter one (i.e., 3-MPA) acts as dilution thiolate.[24,25] Importantly, the latter serves as a spacer to tune the distance among contiguous biorecognition elements, which prevents two neighboring biomolecules to hinder each other in binding the analyte.[24,25] The biofunctionalization process is therefore accomplished by activating the carboxylic moieties of 3-MPA/11MUA SAM through 1-ethyl-3-(3-dimethylaminopropyl)carbodiimide/*N*-hydroxysulfosuccinimide sodium salt (EDC/NHSS) coupling.[20] This enables the antibodies to conjugate to the SAM. Finally, unreacted carboxylic groups are blocked by exposure to an excess of ethanolamine (EA).[26] Consequently, when both long and short thiols are endowed with carboxyl terminal groups, the biomodification does not ensure that the biorecognition element anchoring occurs only on the longer chain SAM sites, leading to a poorly controlled SAM architecture.

A different SAM architecture, replacing 3-MPA (reacted through EDC/NHSS with ethanolamine) with an ad hoc synthesized thiol *N*-(2-hydroxyethyl)-3-mercaptopropanamide (NMPA), was proposed as dilution thiol. This enabled higher SAM architecture control (not depending on EDC/NHSS reaction yield) through hydrogen bonding interactions acting on SAM chains conformational rearrangements. Remarkably, both the NMPA and activated 3-MPA structures enable the formation of an extended hydrogen-bonding network, involving the oxygen of the amide group in one short SAM chain and the hydrogen of the amide group of a neighboring one, which could play a major role in guiding the antibody binding toward the surface. Then, human immunodeficiency virus (HIV-1) antibodies (anti-p24) have been coupled with the gold surfaces modified using the two different mixed SAMs aiming at assessing whether a better control over the conjugation of the biorecognition elements could enable better detection efficacy toward HIV-1 p24 capsid proteins.[27,28] A mm-square wide gold detecting interface modified with the two different mixed SAMs was characterized for the first time with multiparameter surface plasmon resonance (MP-SPR) technique.[29–31] Specifically, SPR has been herein employed to characterize both the efficiency of the two immobilization strategies to anchor the capturing antibodies on the detecting surface and the interaction of the biorecognition element with its cognate ligands and further compared with the results obtained in the presence of bare physisorbed biorecognition elements. Remarkably, an improvement on the anti-p24 surface coverage, along with a more stable coupling of the antibodies to the chemical SAM has been accomplished with the 11-MUA/NMPA SAM modified SPR slide. Density functional theory (DFT) calculations, undertaken to provide a molecular rationale behind the observed experimental data, suggest that the dipole moment of the 11-MUA/NMPA mixed SAM is more effective in electrostatically guiding the anti-p24 antibodies toward the gold detecting interface. This can eventually lead to a layer of antibodies packed to a higher extent onto the 11-MUA/NMPA SAM modified surface as well as a more effective covalent coupling capability of the latter modified surface. Surprisingly, despite the higher anti-HIV1p24 surface coverage obtained with the 11-MUA/NMPA modified surface, the binding efficiency against HIV1 p24 protein is far lower than that obtained with the 11-MUA/3-MPA modified surface. This evidence has been explained considering the supramolecular structure of the mixed SAMs engaged in this study, leading to a peculiar conformational rearrangement of the biolayer. This can directly impact on the degrees of freedom of the capturing antibodies, hindering an efficient interaction with the cognate ligand. This study provides for the first time a clear indication that less tightly packed surfaces lead to more degrees of freedom in antibodies' biofilm and thus a significant enhancement in the antigen binding efficiency of the assay. Moreover, this study provides a physical view of the main competing phenomena affecting the biorecognition events at a biofunctionalized gold detecting interface.

2. Results and Discussion

The SPR generation mechanism relies on the presence of the noble metal thin film which causes partial loss of the reflected laser light, by exciting metal surface electrons. This produces an evanescent wave that propagates along the interface between the dielectric, namely the sample, and the metal layer.[32,33] Being the surface plasma wave mostly confined at the metal–dielectric boundary, it decreases exponentially within the media (dielectric) and increases into both media, with higher field concentration in the dielectric.[33] Hence, the technique is sensitive to any change occurring within the first 300–400 nm of the gold facing the dielectric.[34] Here the local refractive index variations are correlated with the biomolecule interactions that can be inspected. The scanning of the SPR resonance angle allows the *real-time* monitoring of each specimen approaching the metal surface from the dielectric medium. Hence, this setup was used first to characterize the efficacy of the two immobilization strategies herein proposed to deposit the capturing antibodies on the detecting surface and study the interaction of the biorecognition element with its cognate ligands (vide infra). Specifically, an SPR characterization of anti-p24 anchoring on different thiols, namely the 11-MUA/NMPA and the 11-MUA/3-MPA mixed SAMs (at the same molar ratio 1:10), has been performed. In particular, gold-coated glass slides were immersed, immediately after cleaning, in the thiol solutions. A mixture of both 11-MUA/NMPA and 11-MUA/3-MPA in ethanol was used at a final concentration of 10 mM. The slides were rinsed in ethanol, and mounted in the SPR sample holder, to monitor the reaction paths of anti-p24 immobilization. To achieve the correct covalent coupling of antibodies on the mixed SAMs, the established EDC/NHSS method was used.[35,36] Briefly, the

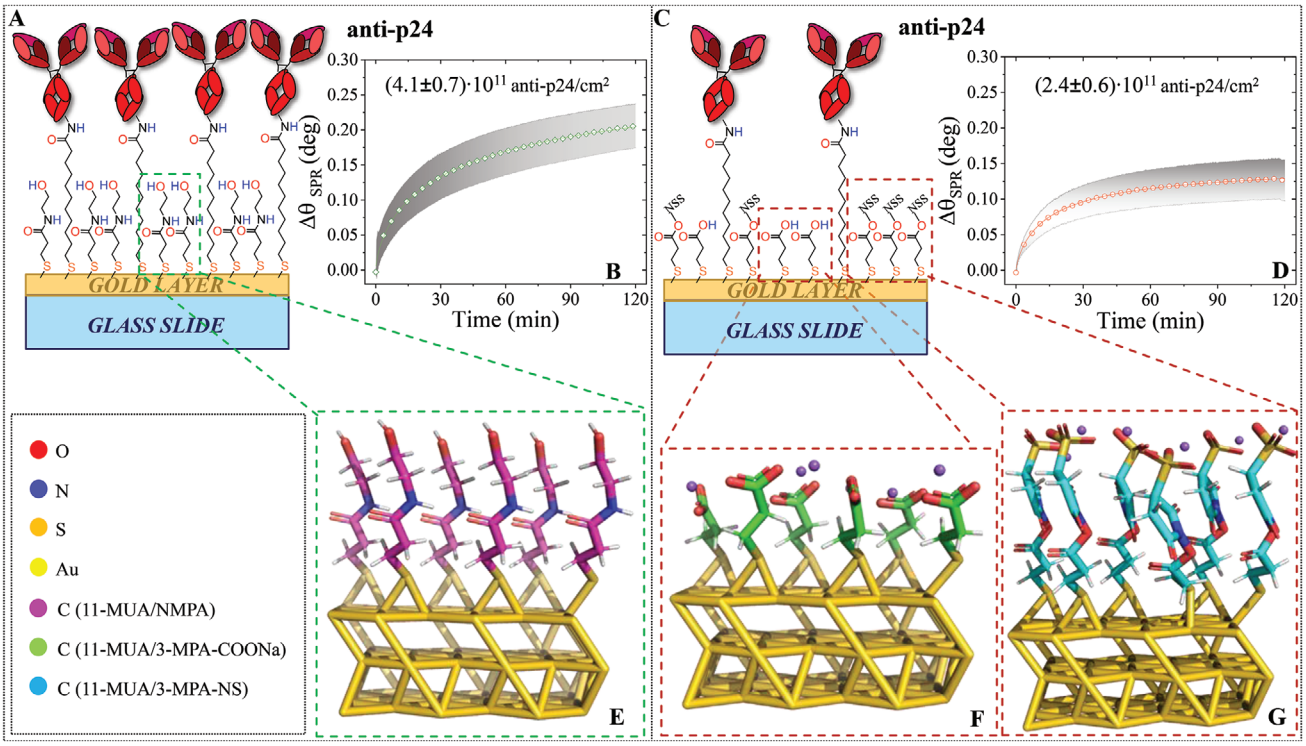

Figure 1. A) Schematic representation of the anti-p24 covalent binding on the mixed SAM (11-MUA/NMPA). B) SPR sensogram of the anti-p24 covalent immobilization through mixed-SAM (11-MUA/NMPA) on the gold SPR slide, reported as average signal over four replicate experiments (green circle) along with their standard deviation (gray shadow). C) Schematic representation of the anti-p24 covalent binding on the mixed SAM (11-MUA/3-MPA). D) SPR sensogram of the anti-p24 covalent immobilization through mixed-SAM (11-MUA/3-MPA) on the gold SPR slide, reported as average signal over four replicate experiments (red circle) along with their standard deviation (gray shadow). DFT optimized structures of the systems used as models of E) 11-MUA/NMPA, F) 11-MUA/3-MPA-COONa, and G) 11-MUA/3-MPA-NSS SAMs. Na+ counterions are depicted as violet spheres while the SAM chains and the gold surface are represented as sticks.

carboxylic terminal groups of the chemical SAM are converted into intermediate reactive species (NHSS, *N*-hydroxysulfosuccinimide esters), which react with the amine groups of the anti-p24 antibody to accomplish its covalent coupling. Then, the ethanolamine saturated solution is injected to deactivate the unreacted esters in an inactive hydroxyethyl amide. Finally, the modified SPR slides have been exposed to bovine serum albumin (BSA) to prevent nonspecific binding.[37] The schematic representations of the anti-p24 covalent binding on the mixed SAMs 11-MUA/NMPA and 11-MUA/3-MPA are depicted in **Figure 1**A–C, respectively. Figure 1C reports two possible configurations achieved during the biolayer formation on the 11-MUA/3-MPA mixed SAM. In fact, the reaction yield of EDC/NHSS on the 3-MPA is lower than an ideal 100% of reacted sites. Tricase et al.[38] previously studied the in-surface activation of SAMs by means of comparative attenuated total reflection infrared (ATR-IR) spectroscopy performed on 3-MPA and NMPA SAMs. The evaluation of the ratio between the amide I and amide II ATR-IR absorption bands was used to build a calibration curve on mixed SAMs holding controlled 3-MPA and NMPA fractions. This allowed to estimate the effective EDC/NHSS reaction yield on the surfaces. Relevantly, the activation of a homogenous 3-MPA SAM, in the same experimental conditions used for the present study, leads to about 66% of activated chains that can eventually react with the biorecognition elements or the saturating ethanolamine solution.[38] Based on this evidence, 40% of the 3-MPA chains in Figure 1C still bears the carboxyl group, after the biofunctionalization protocol has been accomplished.

As a first step, the anti-p24 surface coverage achieved with both mixed SAMs was estimated, analyzing the real-time binding recorded during the antibody immobilization. These experimental responses are shown in Figure 1B–D, for the 11-MUA/NMPA (green circles) and 11-MUA/3-MPA (red circles), respectively. The average SPR angular variations ($\Delta\theta_{SPR}$) versus time shown in Figure 1B–D, evaluated over four different experiments, are reported along with the relative standard deviation (gray shadows).

The anchoring of anti-p24 on the 11-MUA/NMPA mixed SAM, in Figure 1B, leads to an increase of the SPR signal with respect to the one recorded with the anchoring of anti-p24 on the 11-MUA/3-MPA SAM, in Figure 1D. The SPR angular shift can be directly used to quantify the amount on anti-p24 bound to the SAMs, by applying the de Feijter's equation.[30] Indeed, the difference in the SPR angle recorded when the buffer solution is injected into the cell, before and after the antibody immobilization procedure, has been calculated. The values obtained for the modification of both the SAMs are reported in **Table 1**. Noticeably, the response measured on the 11-MUA/NMPA after the anti-p24 anchoring is as high as (0.20 ± 0.04) deg, compared to the 11-MUA/3-MPA SAM which produced an angular shift of (0.13 ± 0.02) deg. Moreover, after

Table 1. Summary of the biofunctionalization procedure, reporting the experimental conditions used for each step of the protocol, along with the time required and the measured SPR angular shift, $\Delta\theta_{SPR}$, for 11-MUA/NMPA and 11-MUA/3-MPA mixed SAMs. The angular shift measured after ethanolamine refers to the antibody layer retained on the surface.

			11-MUA/NMPA	11-MUA/3-MPA
	Reagent	Time	$\Delta\theta_{SPR}$ [deg]	
Activation	EDC/NHSS (0.2 M/0.05 M)	15 min	–	–
Bioconjugation	anti-HIV-1 p24 antibody (50 μg mL^{-1})	2 h	0.20 ± 0.04	0.13 ± 0.02
Bound saturation	Ethanolamine (1 M)	45 min	0.19 ± 0.03	0.11 ± 0.02
Blocking	BSA (100 μg mL^{-1})	1 h	0.026 ± 0.001	0.08 ± 0.01

the saturation with EA a fraction of noncovalently bounded antibodies is rinsed away from the surface.[36] In particular, a decrease of the SPR signal after EA exposure of 15% has been registered when using the 3-MPA-containing SAM, leading that an angular shift of (0.11 ± 0.02) deg. This variation corresponds to an antibodies' surface coverage of (61 ± 16) ng cm^{-2} or equivalently, considering the molecular weight of the antibody, to (2.4 ± 0.6) × 10^{11} anti-p24 cm^{-2}, packed at a density of 2 × 10^3 μm^{-2}. Instead, only 5% of anti-p24 is lost after the EA saturation is performed on the NMPA containing SAM.

In this case, as reported in Table 1, a final angular shift of (0.19 ± 0.03) deg is measured. Consequently, a surface coverage of (102 ± 19) ng cm^{-2} or equivalent to (4.1 ± 0.7) × 10^{11} anti-p24 cm^{-2} has been calculated. The anti-p24 are thus packed at a density as high as 4 × 10^3 μm^{-2}. SPR analysis clearly shows that the 11-MUA/NMPA SAM leads to an increase of 58% of anti-p24 attached to the sensor surface compared to the 11-MUA/3-MPA SAM as well as a more stable coupling of the antibodies to the SAM. Moreover, in the subsequent blocking step in which the biolayer is exposed to the BSA solution, the adsorption of the albumin is enhanced on the SAM encompassing 3-MPA chains. In Table 1 the angular shift, $\Delta\theta_{SPR}$, of (0.08 ± 0.01) deg, measured for BSA adsorption onto the 11-MUA/3-MPA modified slide, is reported. This corresponds to a surface coverage of about (4 ± 1) × 10^{11} albumins cm^{-2}. Instead, the BSA adsorption on the 11-MUA/NMPA mixed SAM reveals a smaller $\Delta\theta_{SPR}$ of (0.026 ± 0.001) deg, from which a 32% lower surface coverage, namely (1.27 ± 0.04) × 10^{11} albumins cm^{-2}, has been estimated. This significant difference between the different amount of BSA adsorbed on the two mixed SAMs can be explained by the higher availability of empty areas left on the not reacted 3-MPA. Also, as reported by Silin et al.,[39] the presence of a homogeneous hydroxyl-terminating SAM could inhibit the nonspecific adsorption of albumin on the surface. This is mainly due to the high hydrophilicity of the OH-terminated SAM, which generally implies lower albumin adsorption compared to COOH-terminated SAMs.[40–42] Thus, the compact layer of NMPA molecules of this mixed SAM could, indeed, prevent albumins from physisorption as suggested by the SPR characterization.

Aiming at providing a rationale behind the different performances shown by the two investigated SAMs, a DFT-based investigation was undertaken. Importantly, based on the adopted experimental conditions, three possible configurations of the dilution thiol composing the SAM were investigated to model the behaviour of 11-MUA/NMPA, depicted in Figure 1E, and 11-MUA/3-MPA, in Figure 1F,G, mixed SAMs undergoing the activation and the succeeding functionalization with the anti-p24. In particular, the possible configurations of the dilution thiols soon after the activation procedure have been investigated. Indeed, after the carboxylic groups have been activated through EDC/NHSS, the surface is exposed to the antibody solution prepared in phosphate buffer saline (PBS) buffered solution (pH 7.4, ionic strength 163 mM). In the case of 11-MUA/3-MPA SAM the antibody approaching the activated SAM could face both a percentage of activated 3-MPA thiols (~ 66%) holding an intermediate succinimide ester (ester-NSS) and a remaining 34% of nonactivated —-COOH,[38] which can be subjected to deprotonation in the PBS pH range used. Noteworthy, both systems can be neutralized by sodium counterions.[43] This is not the case for the 11-MUA/NMPA SAM in which the dilution thiols NMPA is not affected by the activation process, showing off its nonreactive —OH moiety for the entire functionalization process. Thus, both the reacted and unreacted carboxyl-ending thiols (hereinafter referred to as 11-MUA/3-MPA-NSS and 11-MUA/3-MPA-COONa, respectively) and the NMPA SAM were included in the DFT study. Figure 1E–G shows the 3D structures returned by the DFT-based optimization performed with periodic boundary conditions for those thiol configurations, namely 11-MUA/NMPA, MUA/3-MPA-NSS, and 11-MUA/3-MPA-COONa, respectively. As expected, all the structures returned a dipole moment whose *z*-component is positive, thus orienting the positive pole away from the gold surface (**Table 2**). Remarkably, according to the adopted system coordinates, the *z*-axis is perpendicular to the *x*–*y* SAM surface. Nevertheless, a dipole mostly oriented along the *z*-axis was computed starting from the optimized 11-MUA/3-MPA-NSS and 11-MUA/NMPA geometries (*z*-component equal to 77.05 and 77.90 D) while the 11-MUA/3-MPA-COONa system is responsible for a dipole moment mostly oriented along the SAM surface (i.e., along the *x*- and *y*-axis) and having a *z*-component one order of magnitude lower than those returned by the other two systems. These results are relevant to understand

Table 2. Dipole moments (*D*) returned by the DFT optimized structures of the investigated systems.

System	Dipole moment [*D*]		
	x	*y*	*z*
11-MUA/3-MPA-COONa	−33.77	20.74	7.55
11-MUA/3-MPA-NSS	24.60	4.98	77.05
11-MUA/NMPA	−29.18	11.33	77.90

especially the influence of the dipole moment, associated with the SAM in the z direction, in guiding the antibody binding toward the surface. As shown by Emaminejad et al.,[44] the orientation of antibodies can be modulated by the presence of an external electric field to which the molecule gets aligned. This holds true for charged SAMs, which can affect the orientation of antibodies depending on the dipole moment associated to them.[45]

Indeed, the structure of the antibody consists of two identical Fab (fragment antigen-binding) arms and one Fc, forming a "Y"-shaped molecule, as schematically depicted in Figure 1A. The Fab fragments contain the variable regions where the antigen binding occurs. It is worth mentioning that the isoelectric point of the Fab fragment is larger than that of the Fc fragment and the whole antibody.[44,46] Hence, at PBS buffer pH level condition that characterizes the antibody covalent binding on the SAM modified surface, the Fab fragment is positively charged and the Fc fragment is negatively charged.[44] As a result, in this condition, the antibody molecule can be conceived as a dipole, whose vector is pointing from the negatively charged Fc to the positively charged Fab. Therefore, the dipole moment, associated with the 11-MUA/NMPA SAM in the z direction and pointing away from the gold surface, could contribute to controlling and aligning the antibodies with an "end-on" orientation. Thus, the DFT results well support the SPR measurements, providing an indication of a layer of antibodies packed to a higher extent onto the 11-MUA/NMPA SAM modified surface, as well as a more effective covalent coupling capability of the latter modified surface. Remarkably, the electrostatic considerations play a major role in orienting the antibody on the gold surface modified with mixed-SAM where the covalent binding occurs. In fact, covalent binding alone does not ensure an oriented immobilization because a protein's anchoring can occur through many residues simultaneously.[1] For instance, lysine residues, being the most widely used anchoring groups, are abundantly present on the exterior of proteins.

As a further step, the two different biofunctionalized SAMs were characterized in terms of binding efficiency of the immobilized antibodies toward the biorecognition of the HIV-1 p24 antigen. As depicted in **Figure 2**A, along with the 11-MUA/NMPA and 11-MUA/3-MPA SAMs, also the binding efficiency of the bare physisorbed antibodies directly on the gold surface has been assessed. In all those test systems, the biorecognition elements were exposed to the analyte solutions in nominally identical experimental conditions. The HIV-1 p24 solutions at increasing concentrations, ranging from 5×10^{-10} to 1×10^{-6} M, were let to interact with the surfaces for 40 min, then the analyte excess was removed washing with PBS.

The SPR signal recorded after each rinsing was compared to the initial baseline acquired in PBS as well. In Figure 2B the dose-response curves of the SPR assay (angular shift vs nominal ligand concentration) are reported for both the modified SAMs as well as for the physisorbed antibodies. Remarkably, a higher response has been recorded for the binding to the anti-p24 immobilized on the 11-MUA/3-MPA SAM (red squares in Figure 2B), while 85% lower response has been recorded with 11-MUA/NMPA SAM (green circles in Figure 2B). Specifically, 11-MUA/3-MPA SAM exhibited a $\Delta\theta_{SPR}$ of (0.46 ± 0.01) deg, while 11-MUA/NMPA SAM reported (0.068 ± 0.004) deg in a 1 μM HIV-1 p24 solution. The $\Delta\theta_{SPR}$ on the physisorbed antibodies[31] produced a signal of (0.25 ± 0.01) deg (black squares in Figure 2B). These results clearly show that the binding efficiency of the biorecognition elements immobilized on the SPR slide is not directly correlated to the antibodies surface coverage. Indeed, the 11-MUA/NMPA biomodified surface hinders HIV-1 p24 binding, leading to a lower SPR response than that registered with the 11-MUA/3-MPA modified surface. Importantly, the surface coverage obtained in the presence of bare physisorbed anti-p24 antibodies is $(7.5 \pm 0.3) \times 10^{11}$ anti-p24 cm^{-2}, as demonstrated in a previously reported study.[31] Nonetheless, the dose-response curve registered upon exposure HIV-1 p24, shown as black squares in Figure 2B, falls halfway between those obtained when 3-MPA and NMPA-containing SAMs are interrogated. In this perspective, the antigen-binding efficiency of the different biomodified surfaces has been assessed using Equation (1)[47]

$$\%\ \text{binding efficiency} = \frac{\tau_{Ab}}{\tau_{Ag}} \times \frac{\Delta\vartheta_{Ag}}{\Delta\vartheta_{Ab}} \times 100 \quad (1)$$

where $\Delta\theta_{Ag}$ is the angle shift due to p24 antigen binding and $\Delta\theta_{Ab}$ is the response upon anti-p24 antibody immobilization, while τ_{Ab} and τ_{Ag} are the time constant of the association kinetics of the antibodies immobilizations and antigen binding, respectively.[48] These parameters have been extracted from the fitting of the SPR angle shift as a function of time for the anti-p24 immobilization step on the 11-MUA/3-MPA, 11-MUA/NMPA biomodified surface as well as on bare gold, according to Equation (2)[48,49]

$$\Delta\vartheta(t) = \Delta\vartheta_{eq}\left(1 - e^{-t/\tau}\right) \quad (2)$$

where $\Delta\theta_{eq}$ is the equilibrium response, namely the angle shift registered at equilibrium either for the anti-p24 antibody immobilization or p24 antigen binding, while τ is the association time constant registered in the anti-p24 antibody immobilization step or p24 antigen binding. Using the parameters extracted from Equation (2), the binding efficiency has been computed according to Equation (1) for the 11-MUA/NMPA and 11-MUA/3-MPA biomodified surface as well as for the biofunctionalization protocol encompassing direct physisorption of capturing antibodies on gold. The calculated antigen-binding efficiency was as high as 99% for the anti-p24 deposited on 11-MUA/3-MPA SAM, 25% for the physisorbed anti-p24 and 17% for the anti-p24 immobilized on the 11-MUA/NMPA mixed surface.

Moreover, the affinity constant was evaluated for the different biofunctionalization protocols by applying a Hill fitting model, reported in Equation (3)

$$Y = V_{max} \cdot \frac{X^n}{k^n + X^n} \quad (3)$$

to the dose curves of Figure 2B (red and greed full lines).[50,51] The model foresees three parameters, namely the maximum response observed at time = +∞ (V_{max}), the apparent dissociation constant (k), i.e., the ligand concentration, at which half the receptors are bounded to the cognate ligand (if $n = 1$, k equals the K_D) and the Hill's coefficient (n) diverging from 1 for positive ($n > 1$) or negative ($n < 1$) binding cooperativity. Those fitting

ADVANCED MATERIALS INTERFACES
Open Access
www.advmatinterfaces.de

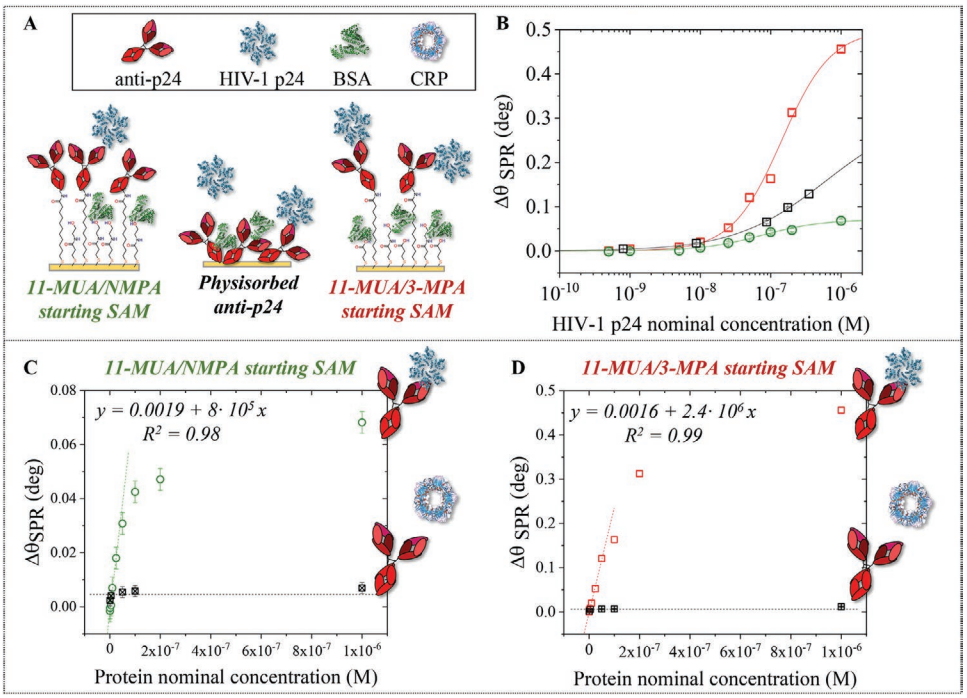

Figure 2. A) Schematic representation of the anti-p24 binding on the mixed SAM (11-MUA/NMPA), directly physisorbed on gold and on the mixed SAM (11-MUA/3-MPA). The binding efficacy of those three surfaces has been tested against HIV-1 p24 antigen. B) Comparison of the dose-curve response (SPR angle shift vs protein nominal concentration) upon exposure to target analyte registered with anti-p24 antibodies deposited on the 11-MUA/NMPA SAM (green circles), directly physisorbed on gold (black squares) and on the 11-MUA/3-MPA SAM (red squares). The points are the average responses along registered for three different experiments, while the error bars are the relative standard deviations. The solid lines are the Hill fitting (see text for more details) performed on the experimental values registered for the three test systems. C) Response registered with the 11-MUA/NMPA SAM (green circles) and nonbinding CRP (black crossed squares). The linear regression on the HIV-1 p24 binding (linear range) is reported as a green-dotted line. D) Response with the 11-MUA/3-MPA SAM (red squares) and nonbinding CRP (black crossed squares). Here the regression of the linear portion of the target analyte response is shown in red-dotted line. For both CRP tests the average control response is shown as a black-dotted line.

parameters, as well as the dissociation constant K_D, estimated as k^n, is reported in **Table 3**. Relevantly, the dissociation constant values obtained for the 11-MUA/3-MPA binding SAM, being $(3.30 \pm 0.04) \times 10^{-9}$ M and the 11-MUA/NMPA, namely $(8.0 \pm 0.3) \times 10^{-8}$ M, are comparable to the dissociation constant values of molecular antibodies against HIV-1 p24 previously reported in literature.[52–54] The dissociation constant of the anti-p24 anchored on the 11-MUA/NMPA SAM is one order of magnitude higher than that registered for anti-p24 segregated onto the 11-MUA/3-MPA SAM. This evidence indicates a higher affinity of the HIV1-p24 proteins for the antibodies anchored on the surface through the SAM encompassing 3-MPA dilution thiols. Moreover, a higher V_{max} value has been achieved with the 3-MPA-comprising SAM, being proportional to the concentration of HIV1-p24 protein that saturates the available binding sites. Additionally, the Hill coefficient, as high as 1.23 ± 0.03, suggests possible positive cooperativity in HIV-1 p24 binding to the surface modified with 11-MUA/3-MPA SAM.

Possible contributions of nonspecific binding were further investigated, designing negative control experiments encompassing the exposure of the modified SPR slides to nonbinding species, namely C-reactive protein (CRP), as previously reported. Those experiments allowed to assess the selectivity of the assay. This protein has been chosen as interferent by reason of the similar molecular weight ($M_{W,CPR}$ = 25 kDa) and structure compared to HIV-1 p24 ($M_{W,p24}$ = 24 kDa) as well as the isoelectric point of tested proteins, which are pI = 6.7 for HIV p24[55] and pI = 5.27 for CRP.[56] Thus, at the pH 7.4 in which the assay has been performed both proteins carry a net negative charge. The analysis was performed on both the modified SAMs, following the same experimental procedure used for the analyte assay. Thus, the two modified surfaces were exposed to increasing concentration of the solution containing the CRP, ranging from 5×10^{-10} to 1×10^{-6} M. Each CPR dilution was kept in contact with the surface for 40 min, and the excess was rinsed with PBS. The buffer level record after each exposure

Table 3. The parameters obtained from the Hill fitting are reported along with their standard error for both the immobilization SAMs. The calculated dissociation constant K_D is reported as well.

Hill fit	V_{max} [deg]	k [M]	n	K_D [M]
11-MUA/3-MPA	0.492 ± 0.004	$(1.28 \pm 0.03) \times 10^{-7}$	1.23 ± 0.03	$(3.30 \pm 0.04) \times 10^{-9}$
11-MUA/NMPA	0.07 ± 0.01	$(8 \pm 2) \times 10^{-8}$	1.0 ± 0.2	$(8.0 \pm 0.3) \times 10^{-8}$

ADVANCED MATERIALS INTERFACES
Open Access
www.advmatinterfaces.de

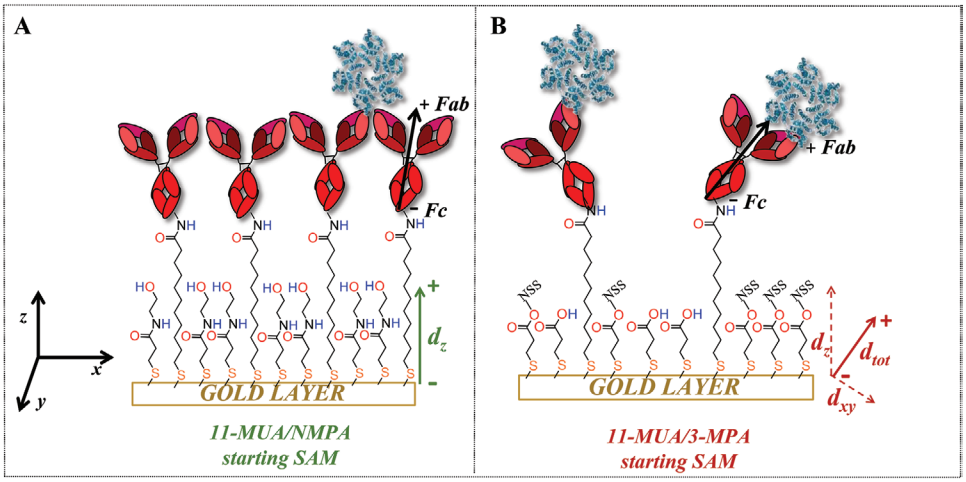

Figure 3. Schematic representation of the anti-p24/HIV1 p24 complex formation on the different biomodified surface. The *xyz* axes are reported in bottom left side of the panel, where according to the adopted system coordinates, the *z*-axis is perpendicular to the *x*–*y* SAM surface. A) Schematic representation of the anti-p24 covalent binding on the mixed SAM (11-MUA/NMPA), along with the DFT computed dipole moment. The NMPA associated dipole moment id depicted as a green arrow oriented along the *z*-axis. B) Schematic representation of the anti-p24 covalent binding on the mixed SAM (11-MUA/3-MPA), comprising both the reacted and unreacted carboxyl-ending thiols, along with the DFT computed dipole moment. The total dipole moment is depicted as a red-full arrow, being the composition of the dipole of the 11-MUA/3-MPA-NSS chains, oriented along the *z*-axis, and the dipole of the 11-MUA/3-MPA-COONa, oriented along the SAM surface (i.e., along the *x*- and *y*-axis), shown as red-dashed arrows.

was compared with the initial baseline acquired in PBS (taken as zero level). The angular shifts registered with the 11-MUA/NMPA SAM as a function of the nominal ligand concentration in linear scale are shown in Figure 2C for both HIV1-p24 sensing (green circles) and nonbinding CRP negative control (black crossed squares) experiments. The linear regression on the HIV-1 p24 binding (linear range) is reported as green-dotted line. Correspondingly, the angular shifts obtained with 11-MUA/3-MPA SAM upon exposure to HIV1-p24 (red squares) and nonbinding CRP (black crossed squares) are reported in Figure 2D. The regression of the linear portion of the target analyte response is shown in red-dotted line. Relevantly, for both the assays (control experiments) a negligible signal has been achieved upon exposure to CRP. Specifically, the selectivity ratio factor ($\Delta\theta_{CRP}/\Delta\theta_{p24}$) has been computed for both assays. Such analysis returned a value of selectivity ratio as low as 0.10 ± 0.01 for the 11-MUA/NMPA modified slide and 0.03 ± 0.01 for the 11-MUA/3-MPA SAM. In both cases, the selectivity ratios are lower than 1, indicating low crossreactivity of the assay. Importantly, the limit of detection (LOD) of the assay has been evaluated for both the biomodified surfaces. In particular, the LOD level was calculated as the average signal of the control experiment (s_{CRP}) plus three times its standard deviation (σ_{CRP}), namely $y_{LOD} = s_{CRP} \pm 3\sigma_{CRP}$.[57] Accordingly, the LOD of the assay has been evaluated using the interpolating linear regressions, shown in Figure 2C,D, leading to LODs of 33 and 6 nM for the 11-MUA/NMPA and 1-MUA/3-MPA biomodified surfaces respectively. The LOD achieved in this study is comparable to those reported in the literature for similar SPR analysis in direct assay configuration, encompassing LOD in the nanomolar range.[27,55,58–62]

The immobilization of anti-HIV1p24 on a gold surface modified with 11-MUA/3-MPA mixed SAM produced an enhancement of the binding efficacy against HIV1 p24 protein compared to the assay encompassing the 11-MUA/NMPA modified surface. In particular, the assay performed using anti-HIV1 p24 capturing antibodies covalently bound to the 11-MUA/3-MPA SAM is more sensitive, it is characterized by an antigen/antibody dissociation constant one order of magnitude lower and a binding efficiency 80% higher than that achieved using 11-MUA/NMPA mixed SAM. All this, despite an anti-p24 surface coverage reduced by a factor 2 with respect to the 11-MUA/NMPA modified surface. Indeed, the partially reacted 3-MPA dilution thiols seem to reduce the total amount of antibody anchored on the surface, by reason of the lower dipole moment found in the z-direction but produced better assay results in terms of antigen binding, as schematically depicted in **Figure 3**A,B. Indeed, the 11-MUA/NMPA dipole moment, oriented along the *z*-axis as shown in Figure 3A, might contribute in guiding the antibody binding toward the surface with an "end-on" orientation leading to a tighter biofilm structure.

On the other hand, as depicted in Figure 3B, the 11-MUA/3-MPA mixed SAM, comprising both the reacted and unreacted carboxyl-ending thiols, is characterized by a total dipole moment, being the composition of the dipole of the 11-MUA/3-MPA-NSS chains, oriented along the *z*-axis, and the dipole of the 11-MUA/3-MPA-COONa, oriented along the SAM surface (i.e., along the x- and y-axis). Consequently, the 11-MUA/3-MPA mixed SAM results in a *z*-component of the dipole moment lower than those returned by the 11-MUA/NMPA. This leads to an antibodies' layer packed to a less extent than that immobilized on the 11-MUA/NMPA, possibly reducing the presence of steric repulsive interactions among the biorecognition elements. This evidence might be ascribable to the different SAMs supramolecular structures,[38,63,64] leading to peculiar conformational rearrangement of biolayer. This can directly impact on the degrees of freedom of the capturing antibodies, hindering an efficient interaction with the cognate ligand. A characterization of mixed SAMs based on IR spectroscopy as well as electrochemical measurements,[64] recently proved that

NMPA SAMs are endowed with a tighter structure with respect to 3-MPA SAM, probably related to high-energetic chain interactions. This might result in a more packed biolayer, dramatically reducing the availability of the binding sites of antibodies capable to bind cognate antigens. On the other hand, 3-MPA SAMs are characterized by a diffuse hydrogen bonding but a relatively low chain length.[64] The latter limits hydrophobic interaction between chains, thus decreasing the stability of compact structures and promoting the formation of pinholes and defects. Consequently, the anti-p24 deposited on the 11-MUA/3-MPA mixed SAM shows better accessibility of the binding sites when exposed to the antigen, due to the higher motility of the biofilm. The latter results from a SAM encompassing a lower level of hydrophobic interaction between short chains while a longer and flexible thiol are used as "spacer-arm" protruding from the surface.[65,66] On the other hand, the anti-p24 biofilm anchored on 11-MUA diluted with well-packed NMPA results in a lowering of the antibodies' degree of freedom, likely reducing the binding affinity between the two biomolecule counterparts (i.e., the antibody and the antigen).[67,68] Such evidence is in agreement with a study by Biscarini and co-workers,[21] predicting that the binding between antigen/antibody pairs might be disfavoured due to the presence of steric repulsive interactions occurring in low mobility and highly packed biofilms.[69]

3. Conclusion

In this study, an MP-SPR technique has been used to gather relevant pieces of information on the binding mechanism of biomolecules on different mixed SAMs. An SPR characterization of anti-p24 anchoring on different thiols, namely the 11-MUA/NMPA and the 11-MUA/3-MPA mixed SAMs (at the same molar ratio 1:10), has been performed. The 11-MUA/NMPA SAM lead to an increase of 58% of anti-p24 attached to the sensor surface as compared to the 11-MUA/3-MPA SAM, as well as a more stable coupling of the antibodies to the SAM. DFT data showed that the 11-MUA/NMPA SAM is characterized by a dipole moment whose *z*-component is positive, thus orienting the positive pole away from the gold surface, and is one order of magnitude higher than that returned by the 11-MUA/3-MPA system. Consequently, the 11-MUA/NMPA SAM is more effective in guiding the antibody binding toward the surface. Thus, the DFT results well support the SPR measurements, providing an indication of a layer of antibodies packed to a higher extent onto the 11-MUA/NMPA SAM modified surface, as well as a more effective covalent coupling capability on such modified SAM surface. Remarkably, despite the higher anti-HIV1p24 surface coverage obtained with the 11-MUA/NMPA modified surface, the binding efficiency against HIV1 p24 protein is 80% lower than that obtained with the 11-MUA/3-MPA SAM modified surface. In particular, the assay performed using anti-HIV1 p24 capturing antibodies covalently bounded to the 11-MUA/3-MPA SAM is more sensitive, selective, and is characterized by an antigen/antibody dissociation constant one order of magnitude lower. This study provides a physical view of the competing phenomena that affect the biorecognition at a biofunctionalized gold detecting interface, in terms of the biorecognition element surface coverage. Such evidence has been explained considering the different supramolecular structures of the mixed self-assembled monolayers engaged in this study, leading to peculiar conformational rearrangement of biolayer. A decrease of sensitivity and selectivity of the SPR assay has been observed by reducing the motility of the anti-HIV1 p24 layer bound to the mixed chemical SAM laying underneath. Importantly, this study provides clear evidence that less tightly packed biomodified surfaces lead to more degrees of freedom of the capturing antibodies, with consequent enhancement in the antigen-binding properties of the assay.

4. Experimental Section

Materials: Mouse monoclonal antibodies for HIV1 p24 (anti-HIV1p24) and the recombinant HIV-1p24 capsid protein (p24, molecular weight 24–26 kDa), expressed in Escherichia coli, were purchased from Abcam (Cambridge, UK). Human C-reactive protein (CRP, molecular weight 118 kDa) was purchased from Sigma-Aldrich. 3-MPA (98%), 11MUA, EA hydrochloride, EDC, NHSS, and BSA (molecular weight 66 kDa) were purchased from Sigma-Aldrich and used without further purification. The synthesis of NMPA was accomplished according to an already reported protocol.[63,70] A PBS solution (Sigma-Aldrich) (phosphate buffer 0.01 M, KCl 0.0027 M, NaCl 0.137 M) was prepared in high-performance liquid chromatography water and used upon filtration on Corning 0.22 µm polyethersulfone membrane. 2-(*N*-morpholino)ethane-sulfonic acid (MES) was purchased from Sigma-Aldrich; a 0.1 M buffer solution was prepared and adjusted at pH 4.8–4.9 with sodium hydroxide solution (NaOH 1 M).

Biofunctionalization of the Gold Slide: An Au coated (≈50 nm) SPR slide (BioNavis Ltd) comprising a chromium adhesion layer (≈2 nm) served as a semi-transparent SPR substrate. Prior to the biofunctionalization, the gold slides have been cleaned in an NH_4OH/H_2O_2 aqueous solution (1:1:5 v v 1) at 80–90 °C for 10 min. The slides were then rinsed in water, dried with nitrogen and treated for 10 min in a UV-ozone cleaner. Substrates were immersed in 10 mM thiol solutions of 11-MUA/NMPA or 11-MUA/3-MPA, both at the same molar ratio 1:10, in degassed ethanol and left overnight in nitrogen atmosphere at 25 °C. Samples were rinsed with ethanol and water prior to the location in the SPR sample-holder, where the slides biofunctionalization has been accomplished. This allowed monitoring in situ and real-time all the following biofunctionalization steps. Specifically, an EDC (200 mM) and NHSS (50 mM) solution in MES acid (pH 4.8, ionic strength 103 mM) was used to accomplish the activation of the thiol terminal groups. Next, the bulk solution was replaced with phosphate buffer solution (PBS, pH 7.4, ionic strength 163 mM). The antibody (anti-HIV-1 p24) solution at a concentration of 50 µg mL^{-1} in PBS was kept in contact with the activated SAMs for 2 h. The surface was then rinsed with PBS and the remaining active sites were quenched with an injection of EA hydrochloride solution at saturating concentration (1 M) for 45 min. This changed the active ester into an inactive hydroxyethyl amide. After, PBS served to rinse again the surface and remove the possible unbounded antibodies. Finally, an albumin solution (BSA, at a concentration 100 µg mL^{-1}) was used to fill potential voids on the SAM surface and to prevent nonspecific binding in the succeeding assay operation. BSA solution was kept in contact with the SPR slide for 1 h, until a plateau in SPR angle shift was recorded.

Surface Plasmon Resonance Characterization: SPR analyses were performed with an MP-SPR Navi 200-L apparatus in the Kretschmann configuration.[71] The gold slide was allotted into the sample-holder, facing the SPR flow-through cell in which the solutions were injected. The SPR apparatus had foreseen that the 0.4 cm^2 gold exposed area was simultaneously inspected at two different points (3 mm apart) to assess the thickness uniformity of the deposited layer. Thus, the thickness of the deposit on the slide was inspected via the evanescent wave generated by two laser beams (both set at $\lambda = 670$ nm) totally reflecting on the Au-covered optical glass.[72] The analysis was carried out by static

ADVANCED MATERIALS INTERFACES
Open Access
www.advmatinterfaces.de

injection in a customized SPR cell encompassing an internal volume of 100 µL. A wide angular range (50°–78°) was measured, with an angular resolution of 0.001°. The variation of the plasmon peak angular response was monitored over time. All the experiments were performed at 24° C. After the biofunctionalization of the SPR slide was accomplished, the modified sensor surface was exposed to the HIV1-p24 protein solutions in PBS, inspecting a concentration range from 5×10^{-10} to 1×10^{-6} M, to assess the antibody binding efficacy.

Computational Details: The CP2K/Quickstep Package[73,74] software program was used for the DFT-based investigation. All calculations were performed using a hybrid Gaussian and plane-wave method, at the Perdew, Burke, and Ernzerhof/double-zeta plus polarization (PBE/DZVP) level of theory and using Goedecker, Teter, and Hutter (GTH) pseudopotentials,[75] together with a 400 Ry plane wave cutoff. The Grimme DFT-D3 method[76] was employed to properly take into account dispersion forces. The starting model systems of the SAMs to be investigated were built following a computational protocol developed elsewhere.[26,77] Specifically, the 111 Au surface was extracted from a bulk gold supercell previously optimized[26] returning a cell parameter $a = 4.152$ Å, close to the experimental one $a_{exp} = 4.078$ Å.[78] The surface was relaxed keeping fixed the gold atoms belonging to the lowest layer in order to take into account bulk constraints. Finally, for each system, six SAM chains were added to the surface following the $(\sqrt{3} \times \sqrt{3})R30°$ configuration, proving to be the most stable one for similar systems.[79–81] The starting models were subjected to geometry optimization, performed at the PBE/DZVP level of theory. Finally, the dipole moments returned by the optimized geometries were computed through a Berry phase calculation.[82] Notice that all the gold atoms were kept fixed during optimization.

Acknowledgements

H2020—Electronic Smart Systems—SiMBiT: Single-molecule bioelectronic smart system array for clinical testing (Grant agreement ID: 824946), ERCStg 2021 "A binary sensor with single-molecule digit to discriminate biofluids enclosing zero or at least one biomarker" (NoOne) (Proposal ID 101040383), "PMGB—Sviluppo di piattaforme meccatroniche, genomiche e bioinformatiche per l'oncologia di precisione"—ARS01_01195—PON "RICERCA E INNOVAZIONE" 2014–2020 projects, Åbo Akademi University CoE "Bioelectronic activation of cell functions", PRIN 17 national project "ACTUAL: At the forefront of Analytical ChemisTry: disrUptive detection technoLogies to improve food safety" (2017RHX2E4), Biosensori analitici usa-e-getta a base di transistori organici autoalimentati per la rivelazione di biomarcatori proteomici alla singola molecola per la diagnostica decentrata dell'HIV (6CDD3786), Research for Innovation REFIN—Regione Puglia POR PUGLIA FESR-FSE 2014/2020, research grant (POR PUGLIA 2/FSE/2020), Center for Colloid and Surface Science, are all acknowledged for partial financial support.

Conflict of Interest

The authors declare no conflict of interest.

Author Contributions

L.S. and P.D. contributed equally to this work. The paper was written through contributions of all authors. All authors have given approval to the final version of the paper.

Data Availability Statement

The data that support the findings of this study are openly available in IDA service at https://my.csc.fi/projects/2005596, reference number 2005596.

Keywords

density functional theory, HIV1 p24 detection, mixed self-assembled monolayers, surface plasmon resonance

Received: January 6, 2023
Revised: February 6, 2023
Published online: March 29, 2023

[1] E. Macchia, F. Torricelli, P. Bollella, L. Sarcina, A. Tricase, C. Di Franco, R. Österbacka, Z. M. Kovács-vajna, G. Scamarcio, L. Torsi, *Chem. Rev.* **2022**, *122*, 4636.
[2] E. Macchia, Z. M. Kovács-Vajna, D. Loconsole, L. Sarcina, M. Redolfi, M. Chironna, F. Torricelli, L. Torsi, *Sci. Adv.* **2022**, *8*, eabo0881.
[3] E. Macchia, L. De Caro, F. Torricelli, C. Di Franco, G. F. Mangiatordi, G. Scamarcio, L. Torsi, *Adv. Sci.* **2022**, *9*, 2104381.
[4] M. Sensi, M. Berto, S. Gentile, M. Pinti, A. Conti, G. Pellacani, C. Salvarani, A. Cossarizza, C. A. Bortolotti, F. Biscarini, *Chem. Commun.* **2021**, *57*, 367.
[5] K. Guo, S. Wustoni, A. Koklu, E. Díaz-Galicia, M. Moser, A. Hama, A. A. Alqahtani, A. N. Ahmad, F. S. Alhamlan, M. Shuaib, A. Pain, I. McCulloch, S. T. Arold, R. Grünberg, S. Inal, *Nat. Biomed. Eng.* **2021**, *5*, 666.
[6] L. Sansone, E. Macchia, C. Taddei, L. Torsi, M. Giordano, *Sens. Actuators, B* **2018**, *255*, 1097.
[7] E. Macchia, R. A. Picca, K. Manoli, C. Di Franco, D. Blasi, L. Sarcina, N. Ditaranto, N. Cioffi, R. Österbacka, G. Scamarcio, F. Torricelli, L. Torsi, *Mater. Horiz.* **2020**, *7*, 999.
[8] M. Magliulo, M. Y. Mulla, M. Singh, E. Macchia, A. Tiwari, L. Torsi, K. Manoli, *J. Mater. Chem. C* **2015**, *3*, 12347.
[9] L. Torsi, A. Dodabalapur, A. J. Lovinger, H. E. Katz, R. Ruel, D. D. Davis, K. W. Baldwin, *Chem. Mater.* **1995**, *7*, 2247.
[10] L. Torsi, F. Marinelli, M. D. Angione, A. Dell'Aquila, N. Cioffi, E. De Giglio, L. Sabbatini, *Org. Electron.* **2009**, *10*, 233.
[11] M. Magliulo, D. De Tullio, I. Vikholm-Lundin, W. M. Albers, T. Munter, K. Manoli, G. Palazzo, L. Torsi, *Anal. Bioanal. Chem.* **2016**, *408*, 3943.
[12] E. Macchia, L. Sarcina, C. Driescher, Z. Gounani, A. Tewari, R. Osterbacka, G. Palazzo, A. Tricase, Z. M. Kovacs Vajna, F. Viola, F. Modena, M. Caironi, F. Torricelli, I. Esposito, L. Torsi, *Adv. Electron. Mater.* **2021**, *7*, 2100304.
[13] M. C. Tanese, D. Fine, A. Dodabalapur, L. Torsi, *Biosens. Bioelectron.* **2005**, *21*, 782.
[14] A. J. Lovinger, D. D. Davis, R. Ruel, L. Torsi, A. Dodabalapur, H. E. Katz, *J. Mater. Res.* **1995**, *10*, 2958.
[15] A. J. Lovinger, D. D. Davis, A. Dodabalapur, H. E. Katz, L. Torsi, *Am. Chem. Soc.* **1996**, *29*, 4952.
[16] F. Rusmini, Z. Zhong, J. Feijen, *Biomacromolecules* **2007**, *8*, 1775.
[17] N. Patel, M. C. Davies, M. Hartshorne, R. J. Heaton, C. J. Roberts, S. J. B. Tendler, P. M. Williams, *Langmuir* **1997**, *13*, 6485.
[18] Y. Sun, J. A. Rogers, *Adv. Mater.* **2007**, *19*, 1897.
[19] G. MacBeath, S. L. Schreiber, *Science* **2000**, *289*, 1760.
[20] B. Holzer, K. Manoli, N. Ditaranto, E. Macchia, A. Tiwari, C. Di Franco, G. Scamarcio, G. Palazzo, L. Torsi, *Adv. Biosyst.* **2017**, *1*, 1700055.
[21] P. A. Manco Urbina, M. Berto, P. Greco, M. Sensi, S. Borghi, M. Borsari, C. A. Bortolotti, F. Biscarini, *J. Mater. Chem. C* **2021**, *9*, 10965.
[22] S. Cotrone, M. Ambrico, H. Toss, M. D. Angione, M. Magliulo, A. Mallardi, M. Berggren, G. Palazzo, G. Horowitz, T. Ligonzo, L. Torsi, *Org. Electron.* **2012**, *13*, 638.
[23] J. W. Lee, S. J. Sim, S. M. Cho, J. Lee, *Biosens. Bioelectron.* **2005**, *20*, 1422.

[24] E. Briand, M. Salmain, J. M. Herry, H. Perrot, C. Compère, C. M. Pradier, *Biosens. Bioelectron.* **2006**, *22*, 440.
[25] D. Ataman Sadık, H. Eksi-Kocak, G. Ertaş, İ. H. Boyacı, M. Mutlu, *Surf. Interface Anal.* **2018**, *50*, 866.
[26] E. Macchia, K. Manoli, B. Holzer, C. Di Franco, M. Ghittorelli, F. Torricelli, D. Alberga, G. F. Mangiatordi, G. Palazzo, G. Scamarcio, L. Torsi, *Nat. Commun.* **2018**, *9*, 3223.
[27] H. H. Nguyen, J. Park, S. Kang, M. Kim, *Sensors* **2015**, *15*, 10481.
[28] U. Jönsson, L. Fägerstam, B. Ivarsson, B. Johnsson, R. Karlsson, K. Lundh, S. Löfås, B. Persson, H. Roos, I. Rönnberg, *BioTechniques* **1991**, *11*, 620.
[29] L. Sarcina, L. Torsi, R. A. Picca, K. Manoli, E. Macchia, *Sensors (Switzerland)* **2020**, *20*, 1.
[30] L. Sarcina, E. Macchia, G. Loconsole, G. D'Attoma, P. Saldarelli, V. Elicio, G. Palazzo, L. Torsi, *Adv. Nanobiomed. Res.* **2021**, *1*, 2100043.
[31] L. Sarcina, G. F. Mangiatordi, F. Torricelli, P. Bollella, Z. Gounani, R. Österbacka, E. Macchia, L. Torsi, *Biosensors* **2021**, *11*, 180.
[32] C. M. Miyazaki, F. M. Shimizu, M. Ferreira, *Nanocharact. Tech.* **2017**, *6*, 183.
[33] J. Homola, *Anal. Bioanal. Chem.* **2003**, *377*, 528.
[34] K. L. M. Moran, D. Lemass, R. O'Kennedy, in *Handbook of Immunoassay Technologies: Approaches, Performances, and Applications*, Elsevier, New York **2018**, pp. 129–156.
[35] S. Sam, L. Touahir, J. Salvador Andresa, P. Allongue, J. N. Chazalviel, A. C. Gouget-Laemmel, C. H. De Villeneuve, A. Moraillon, F. Ozanam, N. Gabouze, S. Djebbar, *Langmuir* **2010**, *26*, 809.
[36] N. J. de Mol, M. J. E. Fischer, in *Surface Plasmon Resonance: Methods in Molecular Biology*, New York **2010**, pp. 55–73, Ch. 3.
[37] J. Y. Lichtenberg, Y. Ling, S. Kim, *Sensors (Switzerland)* **2019**, *19*, 2488.
[38] A. Tricase, D. Blasi, A. Favia, A. Stefanachi, F. Leonetti, G. Colafemmina, L. Torsi, G. Scamarcio, *Appl. Surf. Sci.* **2021**, *559*, 149883.
[39] V. Silin, H. Weetall, D. J. Vanderah, *J. Colloid Interface Sci.* **1997**, *185*, 94.
[40] M. C. L. Martins, C. Fonseca, M. A. Barbosa, B. D. Ratner, *Biomaterials* **2003**, *24*, 3697.
[41] L. Liu, Y. Dai, Y. Qi, *ACS Omega* **2021**, *6*, 16438.
[42] M. Källtorp, A. Carlén, P. Thomsen, J. Olsson, P. Tengvall, *J. Mater. Sci.: Mater. Med.* **2000**, *11*, 191.
[43] N. Goutev, M. Futamata, *Appl. Spectrosc.* **2003**, *57*, 506.
[44] S. Emaminejad, M. Javanmard, C. Gupta, S. Chang, R. W. Davis, R. T. Howe, *Proc. Natl. Acad. Sci. U. S. A.* **2015**, *112*, 1995.
[45] S. Chen, L. Liu, J. Zhou, S. Jiang, *Langmuir* **2003**, *19*, 2859.
[46] J. Zhou, H. K. Tsao, Y. J. Sheng, S. Jiang, *J. Chem. Phys.* **2004**, *121*, 1050.
[47] T. C. Tsai, C. W. Liu, Y. C. Wu, N. A. P. Ondevilla, M. Osawa, H. C. Chang, *Colloids Surf., B* **2019**, *175*, 300.
[48] B. T. Neumann, M. Johansson, D. Kambhampati, W. Knoll, *Adv. Funct. Mater.* **2002**, *16*, 9.
[49] D. Yao, J. Kim, F. Yu, P. E. Nielsen, E. K. Sinner, W. Knoll, *Biophys. J.* **2005**, *88*, 2745.
[50] A. V Hill, *Biochem. J.* **1913**, *7*, 471.
[51] R. Barlow, J. F. Blake, *Trends Pharmacol. Sci.* **1989**, *10*, 440.
[52] E. R. Gray, J. C. Brookes, C. Caillat, V. Turbé, B. L. J. Webb, L. A. Granger, B. S. Miller, L. E. McCoy, M. El Khattabi, C. T. Verrips, R. A. Weiss, D. M. Duffy, W. Weissenhorn, R. A. McKendry, *ACS Infect. Dis.* **2017**, *3*, 479.
[53] R. L. Rich, D. G. Myszka, *Trends Microbiol.* **2003**, *11*, 124.
[54] S. Monaco-Malbet, C. Berthet-Colominas, A. Novelli, N. Battaï, N. Piga, V. Cheynet, F. Mallet, S. Cusack, *Structure* **2000**, *8*, 1069.
[55] L. Zheng, L. Jia, B. Li, B. Situ, Q. Liu, Q. Wang, N. Gan, *Molecules* **2012**, *17*, 5988.
[56] Human CRP Specifications, 2003–2019 Cell Signaling Technology, Inc., https://www.phosphosite.org/proteinAction?id=5126327&showAllSites=true, **n.d**.
[57] F. Allegrini, A. C. Olivieri, *Anal. Chem.* **2014**, *86*, 7858.
[58] S. Tang, I. Hewlett, *J. Infect. Dis.* **2010**, *201*, S59.
[59] P. Fan, X. Li, W. Su, W. Kong, X. Kong, Z. Wang, Y. Wang, C. Jiang, F. Gao, *PLoS One* **2015**, *10*, 1.
[60] E. Hifumi, N. Kubota, Y. Niimi, K. Shimizu, N. Egashira, T. Uda, *Anal. Sci.* **2002**, *18*, 863.
[61] M. Malmqvist, *Curr. Opin. Immunol.* **1993**, *5*, 282.
[62] S. K. Vashist, C. K. Dixit, B. D. MacCraith, R. O'Kennedy, *Analyst* **2011**, *136*, 4431.
[63] D. Blasi, L. Sarcina, A. Tricase, A. Stefanachi, F. Leonetti, D. Alberga, G. F. Mangiatordi, K. Manoli, G. Scamarcio, R. A. Picca, L. Torsi, *ACS Omega* **2020**, *5*, 16762.
[64] A. Tricase, A. Imbriano, N. Ditaranto, E. Macchia, R. A. Picca, D. Blasi, L. Torsi, P. Bollella, *Nanomaterials* **2022**, *12*, 867.
[65] Z. Yang, Y. Chevolot, T. Géhin, V. Dugas, N. Xanthopoulos, V. Laporte, T. Delair, Y. Ataman-Önal, G. Choquet-Kastylevsky, E. Souteyrand, E. Laurenceau, *Langmuir* **2013**, *29*, 1498.
[66] B. Zhang, J. Yu, C. Liu, J. Wang, H. Han, P. Zhang, D. Shi, *RSC Adv.* **2016**, *6*, 50119.
[67] K. E. Nelson, L. Gamble, L. S. Jung, M. S. Boeckl, E. Naeemi, S. L. Golledge, T. Sasaki, D. G. Castner, C. T. Campbell, P. S. Stayton, *Langmuir* **2001**, *17*, 2807.
[68] F. Frederix, K. Bonroy, W. Laureyn, G. Reekmans, A. Campitelli, W. Dehaen, G. Maes, *Langmuir* **2003**, *19*, 4351.
[69] M. Selvaraj, P. Greco, M. Sensi, G. D. Saygin, N. Bellassai, R. D'Agata, G. Spoto, F. Biscarini, *Biosens. Bioelectron.* **2021**, *182*, 113144.
[70] D. Rotili, A. De Luca, D. Tarantino, S. Pezzola, M. Forgione, B. Morozzo della Rocca, M. Falconi, A. Mai, A. M. Caccuri, *Eur. J. Med. Chem.* **2015**, *89*, 156.
[71] E. Kretschmann, H. Raether, *J. Phys. Sci. A* **1968**, *23*, 2135.
[72] E. T. Gedig, in *Handbook of Surface Plasmon Resonance* (Eds: Richard B. M. Schasfoort), The Royal Society of Chemistry, Croydon, UK **2017**, pp. 173–220.
[73] T. D. Kühne, M. Iannuzzi, M. Del Ben, V. V Rybkin, P. Seewald, F. Stein, T. Laino, R. Z. Khaliullin, O. Schütt, F. Schiffmann, D. Golze, J. Wilhelm, S. Chulkov, M. H. Bani-Hashemian, V. Weber, U. Borštnik, M. Taillefumier, A. S. Jakobovits, A. Lazzaro, H. Pabst, T. Müller, R. Schade, M. Guidon, S. Andermatt, N. Holmberg, G. K. Schenter, A. Hehn, A. Bussy, F. Belleflamme, G. Tabacchi, et al., *J. Chem. Phys.* **2020**, *152*, 194103.
[74] CP2K Open Source Molecular Dynamics, https://www.cp2k.org/performance:cirrus-h2o-64 (accessed: September 2021).
[75] S. Goedecker, M. Teter, J. Hutter, *Phys. Rev. B* **1996**, *54*, 1703.
[76] S. Grimme, J. Antony, S. Ehrlich, H. Krieg, *J. Chem. Phys.* **2010**, *132*, 154104.
[77] D. Alberga, G. F. Mangiatordi, A. Motta, O. Nicolotti, G. Lattanzi, *Langmuir* **2015**, *31*, 10693.
[78] J. Zemann, *Acta Crystallogr.* **1965**, *18*, 139.
[79] M. Mrksich, G. M. Whitesides, in *Poly(Ethylene Glycol)*, American Chemical Society, Washington, DC **1997**, pp. 23–361.
[80] Y.-C. Yang, T.-Y. Chang, Y.-L. Lee, *J. Phys. Chem. C* **2007**, *111*, 4014.
[81] Y.-F. Liu, Y.-L. Lee, *Nanoscale* **2012**, *4*, 2093.
[82] K. N. Kudin, R. Car, R. Resta, *J. Chem. Phys.* **2007**, *126*, 234101.